College of Physicians and Surgeons, New York, New York, USA; [3]*The Solomon H. Snyder Department of Neuroscience, Johns Hopkins University School of Medicine, Baltimore, Maryland, USA; and* [4]*Howard Hughes Medical Institute, Johns Hopkins University School of Medicine, Baltimore, Maryland, USA*
[5]*These authors contributed equally to this work.*
[*]*Corresponding author e-mail: ms5664@cumc.columbia.edu*

SUPPLEMENTARY MATERIAL

Supplementary material is linked to the online version of the paper at www.jidonline.org, and at https://doi.org/10.1016/j.jid.2020.06.030.

REFERENCES

Azimi E, Reddy VB, Shade KC, Anthony RM, Talbot S, Pereira PJS, et al. Dual action of neurokinin-1 antagonists on Mas-related GPCRs. JCI Insight 2016;1:e89362.

Bédard PM, Brunet C, Pelletier G, Hébert J. Increased compound 48/80 induced local histamine release from nonlesional skin of patients with chronic urticaria. J Allergy Clin Immunol 1986;78:1121–5.

Borici-Mazi R, Kouridakis S, Kontou-Fili K. Cutaneous responses to substance P and calcitonin gene-related peptide in chronic urticaria: the effect of cetirizine and dimethindene. Allergy 1999;54:46–56.

Che D, Rui L, Cao J, Wang J, Zhang Y, Ding Y, et al. Cisatracurium induces mast cell activation and pseudo-allergic reactions via MRGPRX2. Int Immunopharmacol 2018;62:244–50.

Fujisawa D, Kashiwakura J, Kita H, Kikukawa Y, Fujitani Y, Sasaki-Sakamoto T, et al. Expression of Mas-related gene X2 on mast cells is upregulated in the skin of patients with severe chronic urticaria. J Allergy Clin Immunol 2014;134:622–33.e9.

Ishizaka T, Dvorak AM, Conrad DH, Niebyl JR, Marquette JP, Ishizaka K. Morphologic and immunologic characterization of human basophils developed in cultures of cord blood mononuclear cells. J Immunol 1985;134:532–40.

Lawrence ID, Warner JA, Cohan VL, Hubbard WC, Kagey-Sobotka A, Lichtenstein LM. Purification and characterization of human skin mast cells. Evidence for human mast cell heterogeneity. J Immunol 1987;139:3062–9.

Leysen J, Uyttebroek A, Sabato V, Bridts CH, De Clerck LS, Ebo DG. Predictive value of allergy tests for neuromuscular blocking agents: tackling an unmet need. Clin Exp Allergy 2014;44:1069–75.

McNeil BD, Pundir P, Meeker S, Han L, Undem BJ, Kulka M, et al. Identification of a mast-cell-specific receptor crucial for pseudo-allergic drug reactions. Nature 2015;519:237–41.

Navinés-Ferrer A, Serrano-Candelas E, Lafuente A, Muñoz-Cano R, Martín M, Gastaminza G. MRGPRX2-mediated mast cell response to drugs used in perioperative procedures and anaesthesia. Sci Rep 2018;8:11628.

Ogasawara H, Furuno M, Edamura K, Noguchi M. Novel MRGPRX2 antagonists inhibit IgE-independent activation of human umbilical cord blood-derived mast cells. J Leukoc Biol 2019;106:1069–77.

Roy S, Ganguly A, Haque M, Ali H. Angiogenic host defense peptide AG-30/5C and bradykinin B_2 receptor antagonist icatibant are G protein biased agonists for MRGPRX2 in mast cells. J Immunol 2019;202:1229–38.

Smith CH, Atkinson B, Morris RW, Hayes N, Foreman JC, Lee TH. Cutaneous responses to vasoactive intestinal polypeptide in chronic idiopathic urticaria. Lancet 1992;339:91–3.

Van Gasse AL, Elst J, Bridts CH, Mertens C, Faber M, Hagendorens MM, et al. Rocuronium hypersensitivity: does off-target occupation of the MRGPRX2 receptor play a role? J Allergy Clin Immunol Pract 2019;7:998–1003.

Wedi B, Gehring M, Kapp A. The pseudoallergen receptor MRGPRX2 on peripheral blood basophils and eosinophils: expression and function [e-pub ahead of print] Allergy 2020. https://doi.org/10.1111/all.14213 (accessed 1 February 2020).

CD23 Levels on B Cells Determine Long-Term Therapeutic Response in Patients with Atopic Eczema Treated with Selective IgE Immune Apheresis

Journal of Investigative Dermatology (2021) **141,** 681–685; doi:10.1016/j.jid.2020.05.122

TO THE EDITOR

The complex pathogenesis of atopic eczema involves an impaired epidermal barrier, dysbiosis, and aberrant type 2 immunity (Eyerich and Eyerich, 2018; Werfel et al., 2015) depending on cytokines such as IL-4, IL-5, IL-9, IL-13, and IL-31 as well as eosinophils, basophils, mast cells, and IgE (Eyerich and Eyerich, 2018). This is underpinned by the clinical efficacy of novel therapeutic targets interacting with type 2 immunity such as the IL-4Ra antibody dupilumab (Blauvelt et al., 2017).

The role of IgE in the pathogenesis of atopic eczema is discussed controversially because an intrinsic type of atopic eczema with normal IgE levels exists. However, IgE levels usually correlate well with atopic eczema severity (Aral et al., 2006), and anti-IgE therapies, for example, with omalizumab, a humanized anti-IgE antibody, or selective IgE immune apheresis (IA) are efficient at least in a subgroup of patients. It was shown that cytokine levels in the skin but not circulating IgE correlate with long-term clinical response (Reich et al., 2019). However, the underlying mechanisms are still poorly understood. Therefore, the aim of this study was to identify the mode of action of IA and to define the biomarkers predicting therapeutic outcome.

Experiments were approved by the Paul Ehrlich Institute and by the ethics committee of the Faculty of Medicine of Technical Uninversity of Munich, and written informed patients' consent was obtained. A total of 10 patients with highly elevated serum IgE levels (15.032 ± 10.226 IU/ml) were treated with 10 sessions of IA (Figure 1a and Supplementary Table S1), with a follow-up after 4 weeks. Circulating IgE levels were efficiently reduced after each IA session but were fully restored at follow-up in all the patients (Figure 1b). Nevertheless, some patients showed sustained clinical improvements at follow-up. Patients were clustered into responders and non-responders by means of minimum value of the root mean square distance and were defined by scoring atopic dermatitis (SCORAD) 40 responses (Figure 1b and e). Circulating IgE levels tended to correlate with the SCORAD before IA ($r = 0.619$, $P = 0.056$) and at follow-up; responders

Abbreviations: IA, immune apheresis; SCORAD, scoring atopic dermatitis

Accepted manuscript published online 17 September 2020; corrected proof published online 21 January 2021

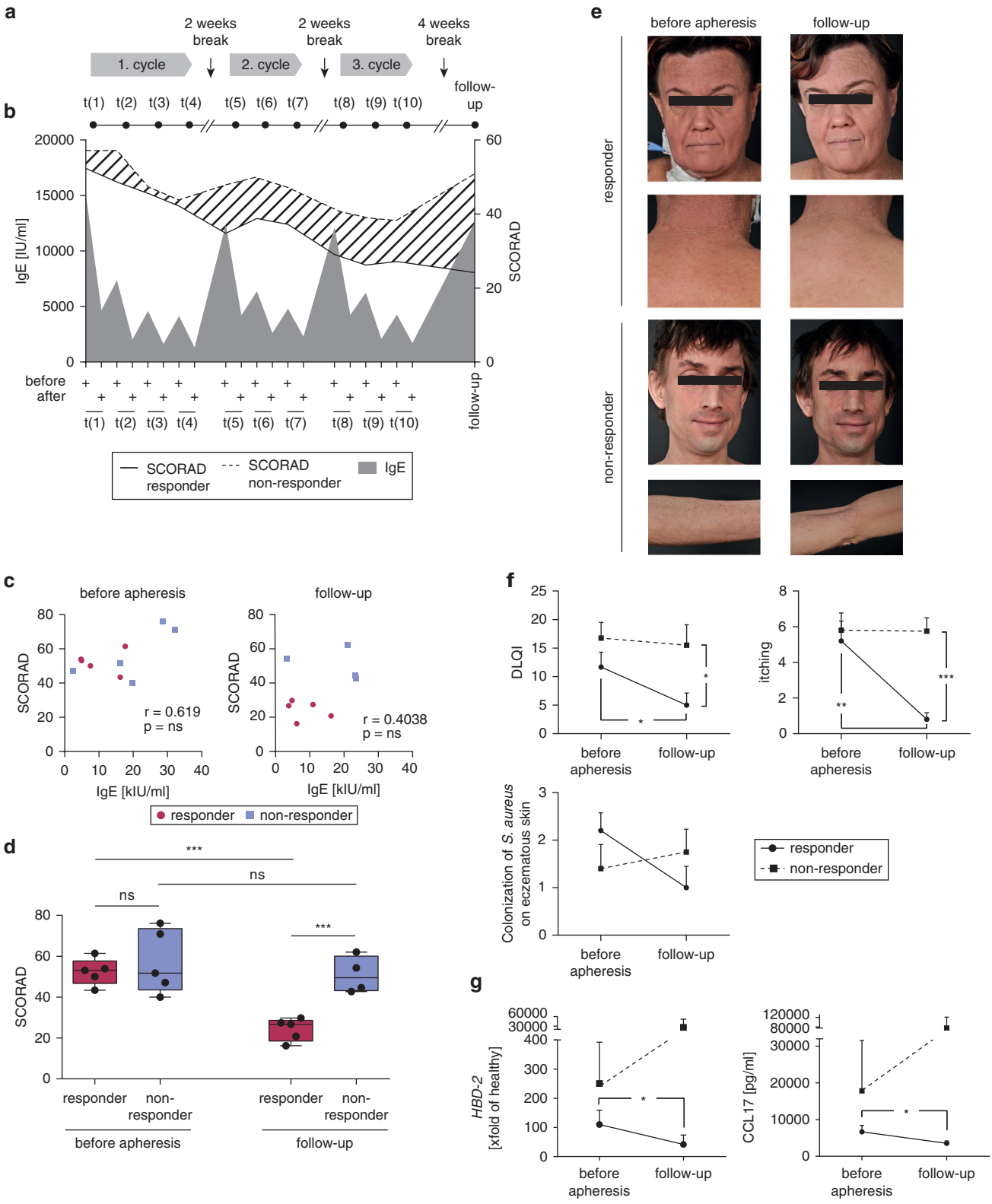

Figure 1. Selective IgE IA leads to long-term clinical response in a subgroup of patients with AE. (**a**) Study design. (**b**) IgE levels (gray area) as well as SCORAD values (solid line: responders, dotted line: non-responders) over time. (**c**) Correlation of SCORAD values (y-axis) and IgE levels (x-axis) in responders (red circles) and non-responders (blue squares) at baseline (left graph) and follow-up (right graph). (**d**) SCORAD values of responders (red box plots) and non-responders (blue box plots) at baseline (left graph) and follow-up (right graph). (**e**) Representative clinical pictures of one responder (upper rows) and one non-responder (lower rows) at baseline (left graphs) and follow-up (right graphs). The patients consented to the publication of the image. (**f**) DLQI scores (upper left graph) and visual analog scale of itch (upper right graph) of the patients (solid line: responders, dotted line: non-responders) and colonization of eczematous skin with *Staphylococcus aureus* at baseline (left) and follow-up (right). (**g**) Lesional cutaneous RNA expression of *HBD-2* (left graph) and serum levels of CCL17 protein (right graph) in the patients (solid line: responders, dotted line: non-responders) at baseline (left) and follow-up (right). AE, atopic eczema; DLQI, Dermatology Life Quality Index; *HBD-2*, human β-defensin 2; IA, immune apheresis; ns, not significant; SCORAD, scoring atopic dermatitis; t, time.

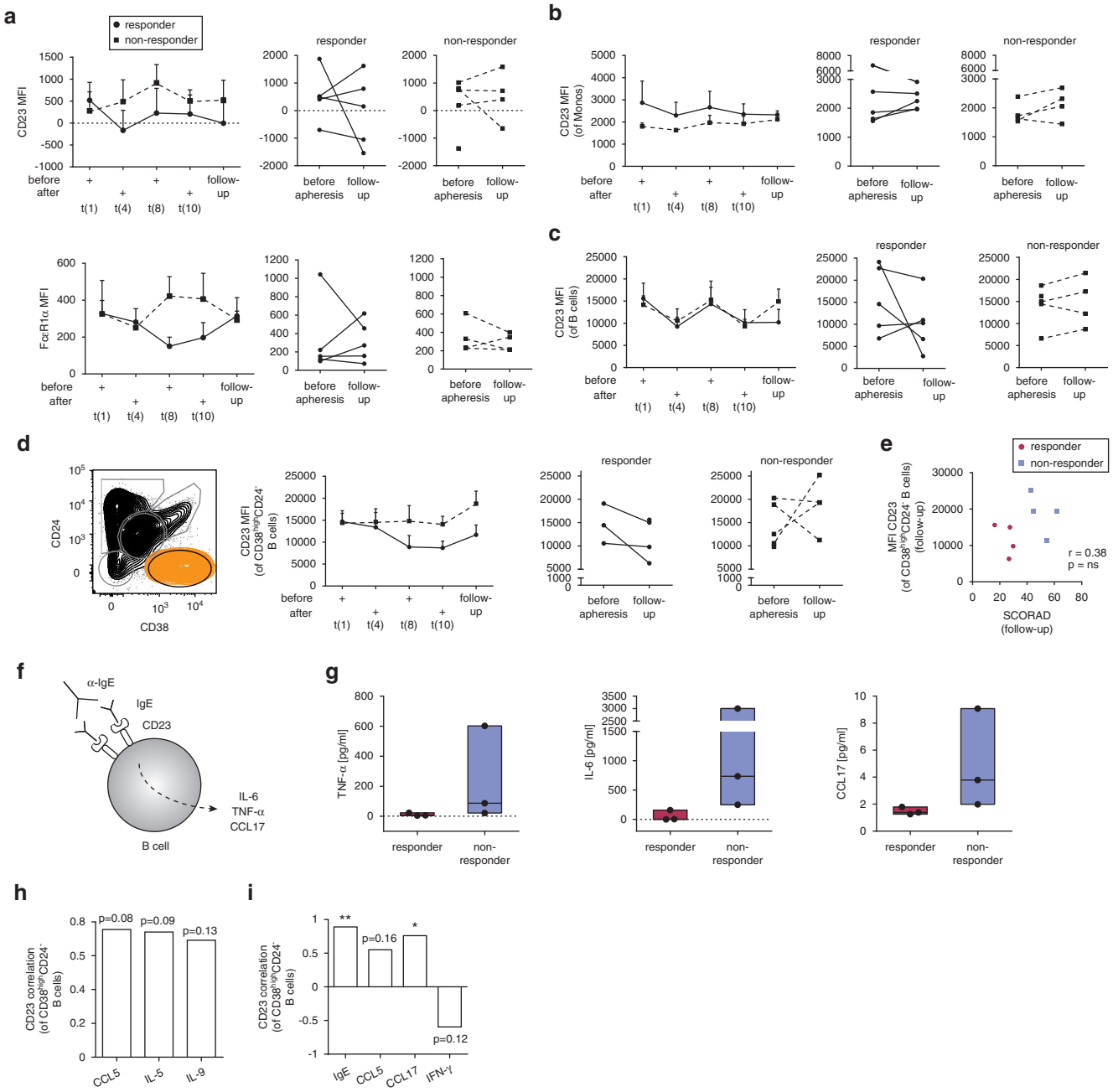

Figure 2. Early and sustained downregulation of CD23 on B-cell populations predicts the long-term response of selective IgE IA. (**a**) Overall CD23 (upper row) and FcεRIα (lower row) levels (MFI) of all immune cell populations in responders (solid line) and non-responders (dotted line) over time (left graphs). Individual changes of CD23 (upper row) and FcεRIα (lower row) levels from baseline to follow-up in responders (middle graphs) and non-responders (right graphs). (**b**) CD23 levels on monocytes in responders (solid line) and non-responders (dotted line) over time (left graph). Individual changes of CD23 levels from baseline to follow-up in responders (middle graph) and non-responders (right graph). (**c**) CD23 levels on pan B cells in responders (solid line) and non-responders (dotted line) over time (left graph). Individual changes of CD23 from baseline to follow-up in responders (middle graph) and non-responders (right graph). (**d**) Gating strategy for B-cell subpopulations (left graph). The middle left graph shows the CD23 levels of $CD38^{high}CD24-$ B cells in responders (solid line) and non-responders (dotted line) over time. Individual changes of CD23 levels from baseline to follow-up in responders (middle right graph) and non-responders (right graph). (**e**) Correlation of CD23 levels on $CD38^{high}CD24-$ B cells in responders (red circles) and non-responders (blue squares) with corresponding SCORAD at follow-up. (**f**) Experimental approach to study CD23 activation on B cells. (**g**) Secretion of TNF-α (left graph), IL-6 (middle graph), and CCL17 (right graph) in pg/ml in the supernatant of α-IgE stimulated B cells isolated from responders (red box plots) and non-responders (blue box plots) at follow-up. (**h**) Correlation of CD23 expression with $CD38^{high}CD24-$ B cells (y-axis) and B-cell–derived cytokines and chemokines. (**i**) Correlation of CD23 expression with $CD38^{high}CD24-$ B cells (y-axis) and serum parameters. IA, immune apheresis; MFI, mean fluorescence intensity; t, time.

showed a trend for lower IgE levels and a significant reduction of SCORAD (Figure 1c and d). Improvement of life quality, pruritus, colonization of eczematous skin with *Staphylococcus aureus* emphasized clinical efficacy of IA in responders (Figure 1f), which was also reflected in decreased serum CCL17 levels and cutaneous levels of human β-defensin 2 (Figure 1g).

Clustering of patients could not detect a distinct responder endotype

regarding cytokine and chemokine levels (Supplementary Figure S1a and b). Apart from the lower CCL17 levels and partially upregulated IFN-γ in responders only on follow-up compared with that on the baseline, no individual mediator indicated clinical response (Supplementary Figure S1b and c). Besides, absolute cell counts of different peripheral immune cells and their relative distribution, their viability, and their stimulatory or proliferative capacity were analyzed to exclude unspecific effects of the IA procedure itself, showing no alterations (Supplementary Figure S2).

To confirm a possible role of IgE in the regulation of IgE receptors expression, we investigated the frequencies of cells positive for low-affinity IgE receptor CD23 and high-affinity IgE receptor FcεRI as well as alterations of receptor densities by flow cytometric analysis in the blood. The overall receptor density of both IgE receptors on immune cells showed a tendency to decrease over time in responders but not in non-responders (Figure 2a and Supplementary Figure S3a). FcεRIα expression did not change significantly on B cells, eosinophils, basophils, and monocytes (Supplementary Figure S3b). However, CD23 expression remained at lower levels at follow-up than at baseline on immune cells. This overall decrease of CD23 was also reflected partially on monocytes but more consistently on pan B cells (Figure 2b and c). The effect of CD23 downregulation was most prominent in the $CD38^{high}CD24-$ B-cell population consisting of plasmablasts and plasma cells (Figure 2d). In this study, a remarkable downregulation of CD23 was observed starting at the end of the first cycle after the fourth IA treatment in responders but not in non-responders. For CD23 levels and SCORAD, a parallel course over the treatment time was observed (Supplementary Figure S3d). Moreover, CD23 levels in responders and non-responders showed a trend to correlate with SCORAD at follow-up (Figure 2e).

To independently prove the functional relevance of IgE-mediated decrease of CD23 expression on B cells, circulating B cells were isolated at follow-up and stimulated with α-IgE (Figure 2f).

The B cells obtained from responders secreted less TNF-α (14.133 ± 9.303 vs. 236.89 ± 183.718 pg/ml, $P = 0.4171$), IL-6 (53.825 ± 52.174 vs. 1,328.195 ± 847.546 pg/ml, $P = 0.2078$), and CCL17 (1.477 ± 0.16 vs. 4.95 ± 2.131 pg/ml, $P = 0.1794$) than those from non-responders (Figure 2g).

Further proinflammatory (CXCL8, G-CSF, VEGF) and type 2 immunity (CCL5, IL-5, IL-9) markers were additionally secreted in lower amounts by B cells obtained from the responders (Supplementary Figure S4). Besides, the B cell derived CCL5 ($r = 0.755$; $P = 0.083$), IL-5 ($r = 0.741$; $P = 0.092$), and IL-9 ($r = 0.692$; $P = 0.128$) showed a positive correlation with CD23 expression on B cells (Figure 2h). Of note, CD23 levels on the B cells significantly correlated with serum IgE level ($r = 0.892$; $P = 0.003$) and showed positive correlation with serum CCL5 ($r = 0.551$; $P = 0.157$) and CCL17 ($r = 0.76$; $P = 0.029$), whereas serum IFN-γ correlated negatively ($r = -0.595$; $P = 0.120$) (Figure 2i).

CD23 plays an important role at the interface of B and T cells by enhancing IgE-mediated antigen uptake, processing, and presentation to T cells (Kehry and Yamashita, 1989). Besides, CD23 controls the secretion of immune mediators by B cells. In line with this, neutralization of CD23 using the mAb lumiliximab resulted in inhibited antigen-specific lymphocyte proliferation and reduced secretion of proinflammatory cytokines as well as type 2 cytokines such as IL-5 (Poole et al., 2005). Correlations of IgE and CD23 expression on B cells have already been described earlier (Czarnowicki et al., 2016; Selb et al., 2017). Moreover, we showed CD23-dependent TNF-α secretion of B cells as well as the secretion of GM-CSF and IL-6, which was decreased in the responder group. TNF-α induces CCL17 secretion by keratinocytes (Yu et al., 2002), and GM-CSF and IL-6 can trigger CCL17 production in dendritic cells (Achuthan et al., 2016); diminished secretion of those mediators by B cells from responders might contribute to decreased serum CCL17 level. Several feedback loops control the expression of CD23 on B cells, for example, circulating IgE (Sherr et al., 1989), as well as T cell cytokines. In the latter case, CD23 is induced by type 2 cytokine IL-4 but downregulated by IFN-γ (Prinz et al., 1990).

Our study certainly has limitations. First, owing to the complex and time-consuming technique of IA with patients spending several hours over several weeks stationary in the clinic, it was not possible to establish a placebo group. Owing to the same reason, the study cohort is rather small. Therefore, wherever possible, findings were validated by measuring different parameters or by performing in vitro approaches. Although these data need to be interpreted carefully regarding these limitations, we think that our study provides interesting evidence for the mode of action as well as for a biomarker of IA, which could be a starting point for further studies.

In this study, we show that IA acts through the downregulation of the low-affinity IgE receptor CD23 in a distinct B-cell subset exclusively in clinical responders. This resulted in lower secretion of IL-6, TNF-α and CCL5, cytokines, and chemokines that are involved in type 2 immunity. By means of these findings, we suggest that CD23 is a regulator of long-term type 2 immune responses and can be used as an early biomarker in determining sustained clinical response to IA or possibly type 2–directed therapies in general.

Data availability statement

The authors declare that all the data supporting the findings of this study are available within the manuscript or are available from the corresponding authors upon request.

ORCIDs

Jenny Thomas: http://orcid.org/0000-0002-6386-7352
Rosi Wang: http://orcid.org/0000-0001-5235-516X
Richa Batra: http://orcid.org/0000-0003-3708-0086
Alexander Böhner: http://orcid.org/0000-0003-1590-0805
Natalie Garzorz-Stark: http://orcid.org/0000-0002-7409-7883
Bernadette Eberlein: http://orcid.org/0000-0003-4509-6491
Fabian Theis: http://orcid.org/0000-0002-2419-1943
Tilo Biedermann: http://orcid.org/0000-0002-5352-5105
Carsten Schmidt-Weber: http://orcid.org/0000-0002-3203-8084
Alexander Zink: http://orcid.org/0000-0001-9313-6588
Kilian Eyerich: http://orcid.org/0000-0003-0094-2674

Stefanie Eyerich: http://orcid.org/0000-0002-1166-2355

CONFLICT OF INTEREST

The authors state no conflict of interest.

ACKNOWLEDGMENTS

We thank Jana Sänger for excellent technical support. This study was performed with samples of the Biobank Biederstein of the Technical University of Munich (Munich, Germany). This study was supported by a grant of Miltenyi Biotec (Bergisch Gladbach, Germany).

AUTHOR CONTRIBUTIONS

Conceptualization: KE, SE, AZ; Data Curation: JT, RW; Formal Analysis: JT, RW, RB, FT; Funding Acquisition: KE, AZ; Investigation: JT, RW; Methodology: JT, KE, SE, AZ; Project Administration: JT, KE, SE, AZ; Resources: KE, SE, AZ, BE, TB, CSW; Software: RB, FT; Supervision: JT, KE, SE, AZ; Validation: JT, RW, KE, SE, NGS, AB; Visualization: JT, RW, KE, SE, NGS; Writing - Original Draft Preparation: JT, RW, KE, SE; Writing - Review and Editing: KE, SE, AZ, BE, TB, CSW

Jenny Thomas[1,6], Rosi Wang[2,6,*], Richa Batra[3], Alexander Böhner[2], Natalie Garzorz-Stark[2], Bernadette Eberlein[2], Fabian Theis[3,4], Tilo Biedermann[2], Carsten Schmidt-Weber[1], Alexander Zink[2], Kilian Eyerich[2,5,7] and Stefanie Eyerich[1,7]

[1]ZAUM—Center of Allergy and Environment, Technical University and Helmholtz Center Munich, Munich, Germany; [2]Department of Dermatology and Allergy, Technical University of Munich, Munich, Germany; [3]Institute of Computational Biology, Helmholtz Center Munich, Neuherberg, Germany; [4]Department of Mathematics, Technical University of Munich, Garching, Germany; and [5]Unit of Dermatology and Venerology, Department of Medicine, Karolinska Institute, Karolinska University Hospital, Stockholm, Sweden

[6]These authors contributed equally to this work.

[7]These authors contributed equally to this work.

[*]Corresponding author e-mail: rosi.wang@tum.de

SUPPLEMENTARY MATERIAL

Supplementary material is linked to the online version of the paper at www.jidonline.org, and at https://doi.org/10.1016/j.jid.2020.05.122.

REFERENCES

Achuthan A, Cook AD, Lee MC, Saleh R, Khiew HW, Chang MW, et al. Granulocyte macrophage colony-stimulating factor induces CCL17 production via IRF4 to mediate inflammation. J Clin Invest 2016;126:3453–66.

Aral M, Arican O, Gul M, Sasmaz S, Kocturk SA, Kastal U, et al. The relationship between serum levels of total IgE, IL-18, IL-12, IFN-gamma and disease severity in children with atopic dermatitis. Mediators Inflamm 2006;2006:73098.

Blauvelt A, de Bruin-Weller M, Gooderham M, Cather JC, Weisman J, Pariser D, et al. Long-term management of moderate-to-severe atopic dermatitis with dupilumab and concomitant topical corticosteroids (LIBERTY AD CHRONOS): a 1-year, randomised, double-blinded, placebo-controlled, phase 3 trial. Lancet 2017;389:2287–303.

Czarnowicki T, Gonzalez J, Bonifacio KM, Shemer A, Xiangyu P, Kunjravia N, et al. Diverse activation and differentiation of multiple B-cell subsets in patients with atopic dermatitis but not in patients with psoriasis. J Allergy Clin Immunol 2016;137:118–29.e5.

Eyerich K, Eyerich S. Immune response patterns in non-communicable inflammatory skin diseases. J Eur Acad Dermatol Venereol 2018;32:692–703.

Kehry MR, Yamashita LC. Low-affinity IgE receptor (CD23) function on mouse B cells: role in IgE-dependent antigen focusing. Proc Natl Acad Sci USA 1989;86:7556–60.

Poole JA, Meng J, Reff M, Spellman MC, Rosenwasser LJ. Anti-CD23 monoclonal antibody, lumiliximab, inhibited allergen-induced responses in antigen-presenting cells and T cells from atopic subjects. J Allergy Clin Immunol 2005;116:780–8.

Prinz JC, Baur X, Mazur G, Rieber EP. Allergen-directed expression of Fc receptors for IgE (CD23) on human T lymphocytes is modulated by interleukin 4 and interferon-gamma. Eur J Immunol 1990;20:1259–64.

Reich K, Hartjen A, Reich J, Schröder J, Steingrube N, Bresch M, et al. Immunoglobulin E-selective immunoadsorption reduces peripheral and skin-bound immunoglobulin E and modulates cutaneous IL-13 expression in severe atopic dermatitis. J Invest Dermatol 2019;139:720–3.

Selb R, Eckl-Dorna J, Neunkirchner A, Schmetterer K, Marth K, Gamper J, et al. CD23 surface density on B cells is associated with IgE levels and determines IgE-facilitated allergen uptake, as well as activation of allergen-specific T cells. J Allergy Clin Immunol 2017;139:290–99.e4.

Sherr E, Macy E, Kimata H, Gilly M, Saxon A. Binding the low affinity Fc epsilon R on B cells suppresses ongoing human IgE synthesis. J Immunol 1989;142:481–9.

Werfel T, Heratizadeh A, Niebuhr M, Kapp A, Roesner LM, Karch A, et al. Exacerbation of atopic dermatitis on grass pollen exposure in an environmental challenge chamber. J Allergy Clin Immunol 2015;136:96–103.e9.

Yu B, Koga T, Urabe K, Moroi Y, Maeda S, Yanagihara Y, et al. Differential regulation of thymus- and activation-regulated chemokine induced by IL-4, IL-13, TNF-alpha and IFN-gamma in human keratinocyte and fibroblast. J Dermatol Sci 2002;30:29–36.

Identification of a Mosaic Activating Mutation in *GNA11* in Atypical Sturge-Weber Syndrome

Journal of Investigative Dermatology (2021) **141,** 685–688; doi:10.1016/j.jid.2020.03.978

TO THE EDITOR

Sturge-Weber syndrome (SWS) (Online Mendelian Inheritance in Man #185300) is a capillary malformation condition (Bichsel and Bischoff, 2019; Comi, 2015). Affected regions include the skin (typically with facial cutaneous vascular malformations called port-wine birthmarks), brain (often resulting in seizures, intellectual disability, and recurrent stroke-like episodes), and eye (often causing glaucoma). We (Shirley et al., 2013) and others (Frigerio et al., 2015; Nakashima et al., 2014) reported that 90% of individuals with SWS or nonsyndromic port-wine birthmarks have a mosaic, activating mutation in *GNAQ*, encoding Gαq. The same mutation at other sites on the skin can also result in cutaneous vascular and soft tissue overgrowth and underlying malformations (Gao et al., 2017; Ma et al., 2018; Tan et al., 2016). Identification of other noncanonical pathogenic mutations may elucidate further the pathophysiology of SWS and/or port-wine birthmarks and define genetic subtypes.

Based on targeted next-generation sequencing, we identified five individuals with SWS and/or port-wine birthmarks who were negative for

Abbreviations: MAF, minor allele frequency; SWS, Sturge-Weber syndrome

Accepted manuscript published online 7 August 2020; corrected proof published online 24 September 2020

SUPPLEMENTARY MATERIALS AND METHODS

Patient characteristics and study design

A total of 10 patients with atopic eczema were recruited for the study. The diagnosis was based on the criteria of Hanifin and Raijka combined with clinical history, symptoms, and clinical and histologic examination. Individuals with systemic immune-suppressive therapy were excluded from the study. Patient characteristics are summarized in Supplementary Table S1. The study was conducted according to the Helsinki declaration; written informed consent was obtained from every participant before study inclusion, and the study was approved by the local ethical committee (reference number 2486/09). Patients received a total of 10 selective IgE immune apheresis (IA) sessions using TheraSorb-IgE LIFE 18 (Miltenyi Biotec, Bergisch Gladbach, Germany) that were performed in 3 intervals with selective IgE IA on 3 or 4 consecutive days. A follow-up examination was performed 4 weeks after the last treatment. Scoring atopic dermatitis was used to determine the disease severity before every treatment day and at follow-up. The total IgE levels were measured using automated systems (Phadia, Freiburg, Germany) before and after each treatment day and at follow-up. Six-millimeter punch biopsies were obtained under local anesthesia before selective IgE IA and at follow-up and used for histologic analysis and RNA isolation. *Staphylococcus aureus* colonization was determined by the culture of microbiological swaps before selective IgE IA and at follow-up.

Blood cell counts

Blood basophil, eosinophil, neutrophil, monocyte, and lymphocyte numbers were determined by using an automated hematocytometer (Advia 120 Hematology System, Siemens, Munich, Germany).

Flow cytometry

After lysis of red blood cells, peripheral blood cells were stained with Viobility 405/520 Fixable Dye (Miltenyi Biotec) to exclude dead cells from analysis. After incubation with Human BD Fc Block (Becton, Dickinson and Company, Franklin Lakes, NJ), cells were stained for 30 minutes at 4 °C using fluorochrome-labeled antibodies binding to cell-surface markers: BV421-CD24 (clone ML5), BV605-CD19 (clone SJ25C1), BV650-CD14 (clone M5E2), APC-Cy7-CD16 (clone 3G8), FITC-CD38 (clone HIT1) (all from BD Biosciences, Heidelberg, Germany), PE-FcεRIα (clone CRA1), PE-CD138 (clone 44F9), APC-CD193 (clone 5E8.4), VioBright FITC-CD19 (clone LT19), PE-Vio770-CD23 (clone M-L23.4), APC-CD27 (clone REA499), PE-CD32 (clone 2E1), APC-Vio770-CD3(clone BW264/56), VioBlue-CD3 (clone BW264/56), PE-Vio615-CD56 (clone REA196), and PerCP-Vio700-CD64 (clone REA196) (all from Miltenyi Biotec). Cells were acquired with an LSRFortessa flow cytometer (BD Biosciences) and analyzed using FlowJo software, version 10 (FlowJo, LLC, Ashland, Oregon).

Immune cells were differentiated on the basis of the expression of certain surface markers as follows: Basophils (CCR3+SSC^{low}), eosinophils (CCR3+SSC^{high}), neutrophils (CCR3−SSC^{high}), monocytes (CD14+), T cells (CD3+), NK T cells (CD3+CD56+), NK cells (CD3−CD56+), and B cells (CD19+). The CD19+ B-cell population was further subdivided into five subsets according to their CD24 and CD38 expression, two markers that are expressed on all B cells but differentially regulated during B-cell development. This well-established approach enables to distinguish CD24+CD38− primarily memory B cells, CD24^{int}CD38^{int} mature naive B cells, CD24^{high}CD38^{high} transitional B cells (also regulatory B cells), CD24−CD38+ plasmablasts (also plasma cells), and CD24−CD38− new memory B cells. All immune cell populations were further analyzed for their IgE receptor expression profile (FceRI and CD23).

Basophil activation test

Basophil activation tests from whole blood were performed by using the Bühlmann Flow CAST assay kit (BÜHLMANN Laboratories AG, Schönenbuch, Switzerland), according to the manufacturer's instructions. In brief, whole blood was stimulated with anti-FcεRI, fMLP, or left unstimulated as control with parallel staining for surface CCR3 and CD63. After erythrocyte lysis, basophil activation was detected by flow cytometry.

PBMC isolation and stimulation

PBMCs were isolated by density gradient centrifugation. Briefly, EDTA blood was diluted at 1:2 with PBS (without calcium and magnesium) and carefully layered on lymphoprep solution (Stemcell Technologies, Vancouver, Canada). After a centrifugation step, the PBMC band was collected and washed with PBS (without calcium and magnesium, supplemented with 5 mM EDTA). PBMCs were cultured either in medium (RPMI supplemented with 5% human serum, 2 mmol/l glutamine, 1 mmol/l sodium pyruvate, 1% nonessential amino acids, and 1% penicillin and/or streptomycin) alone or stimulated with plate-bound anti-CD3 and soluble anti-CD28 (both 0.75 μg/ml) mAbs or phytohemagglutinin (1 ng/ml), respectively, for 72 hours at 37 °C and 5% carbon dioxide.

B-cell isolation and stimulation

B cells were isolated from PBMCs with magnetic beads using a Pan B cell kit (Miltenyi Biotec) yielding an untouched cell population containing all B-cell subpopulations. B cells were cultured either in medium (RPMI supplemented with 5% human serum, 2 mmol/l glutamine, 1 mmol/l sodium pyruvate, 1% nonessential amino acids, and 1% penicillin and/or streptomycin) alone or stimulated with 150 μg/ml α-IgE (Dako, Glostrup, Denmark) for 48 hours at 37 °C and 5% carbon dioxide. Where indicated, B cells were preincubated with 2 μg/ml recombinant IgE (EMD Millipore, Billerica, MA) for 6 hours. After removing supernatant with unbound IgE, spiked B cells were stimulated with 150 μg/ml α-IgE (Dako) for 48 hours at 37 °C and 5% carbon dioxide.

RNA isolation and real-time PCR

Total RNA was isolated by using miRNeasy Mini Kit (Qiagen, Hilden, Germany), according to the manufacturer's instructions. The RNA yield and quality were determined with a NanoDrop ND1000 UV-vis Spectrophotometer (Thermo Fisher, Waltham, MA).

For amplification of genes of interest, cDNA was transcribed with the High Capacity cDNA Reverse Transcript

Amplification Kit (Applied Biosystems, Foster City, CA), according to the manufacturer's instructions. The primers amplifying the genes of interest were designed by using the publicly accessible Primer-BLAST software (https://www.ncbi.nlm.nih.gov/tools/primer-blast/). Real-time PCR reactions were performed in 384-well plates with 10 ng cDNA per well plate using the Fast Start SYBR Green Master Mix (Roche Applied Science, Penzberg, Germany), and fluorescence was monitored with the ViiA7 Real-Time PCR machine (Applied Biosystems). The expression of transcripts was normalized to the expression of 18S ribosomal RNA as a housekeeping gene. Relative quantification was determined according to the following formula: relative quantification $= 2^{-\Delta\Delta Ct}$. Primers used were as follows: 18S forward 5′-GTAACCCGTTGAACCCCATT-3′; 18S reverse 5′-CCATCCAATCGGTAGTAGCG-3′; human β-defensin 2 forward 5′-AAGGTGGAAGGCTTGATGTCC-3′, reverse 5′- TACCACCAAAAACACCTGGAA-3′; Ki67 forward 5′-GCAAGCACTTTGGAGAGCAAAT-3′, reverse 5′-GTCCTCAGCCTTCTTTGGATT-3′.

ELISA and Luminex

Cytokine levels from cell-culture supernatant were measured by sandwich ELISA for IL-6, TNF-α, and CCL17 using commercially available kits following the manufacturer's instructions (IL-6 from Becton, Dickinson and Company; TNF-α and CCL17 from Research and Diagnostic Systems, Minneapolis, MN).

Serum cytokine levels were measured with the Bio-Plex Pro Human Cytokine 27-plex Assay (Bio-Rad Laboratories, Hercules, CA), according to the manufacturer's instructions.

Statistics

Heatmaps were generated using the R package pheatmap. Data were log transformed and scaled per cytokine. Statistical analysis was performed using GraphPad Prism 7.00 software (GraphPad Software, La Jolla, CA). Variables were correlated using Pearson rank correlation. Lines show the mean values with SEM. Box plots extend from 25th to 75th percentile with whiskers plotted to the minimum and maximum showing all data points. The line in the middle of the box is plotted at the median. Statistical differences were calculated by paired or unpaired *t*-tests and expressed as *P*-values: $P \geq 0.05$ = not significant; $^{*}P < 0.05$; $^{**}P < 0.01$; $^{***}P < 0.001$.

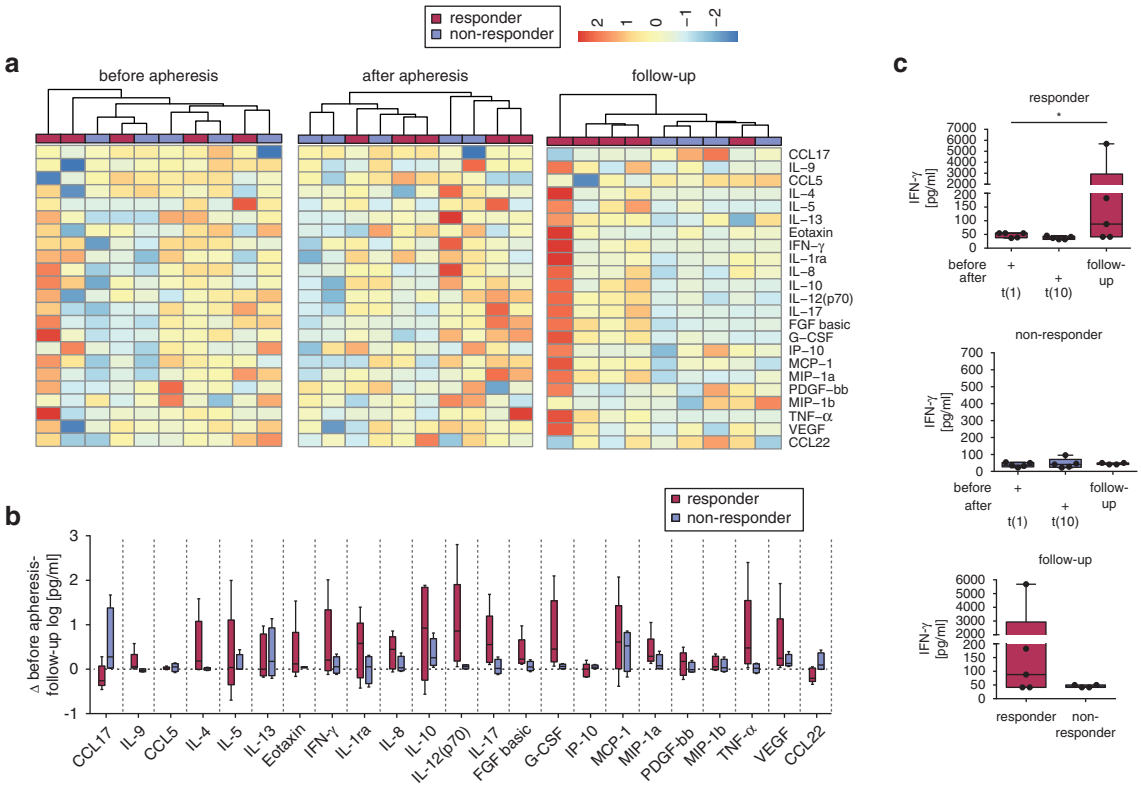

Supplementary Figure S1. Selective IgE IA does not selectively affect soluble immune mediators. (**a**) Hierarchical clustering of patients (first-row red box: responder, blue box: non-responder) according to levels of 23 soluble immune mediators in circulation at baseline (left graph), directly after 10 selective IgE IA procedures (middle graph), and at follow-up (right graph). (**b**) Change of immune mediator concentrations in the circulation at follow-up as compared with those of the baseline, stratified for responders (red) and non-responders (blue). (**c**) Serum IFN-γ levels over time (x-axis) in responders (upper graph, red box plots) and non-responders (middle graph, blue box plots). Comparison of serum IFN-γ levels at follow-up between responders (red box plots) and non-responders (blue box plots) (lower graph). IA, immune apheresis; t, time.

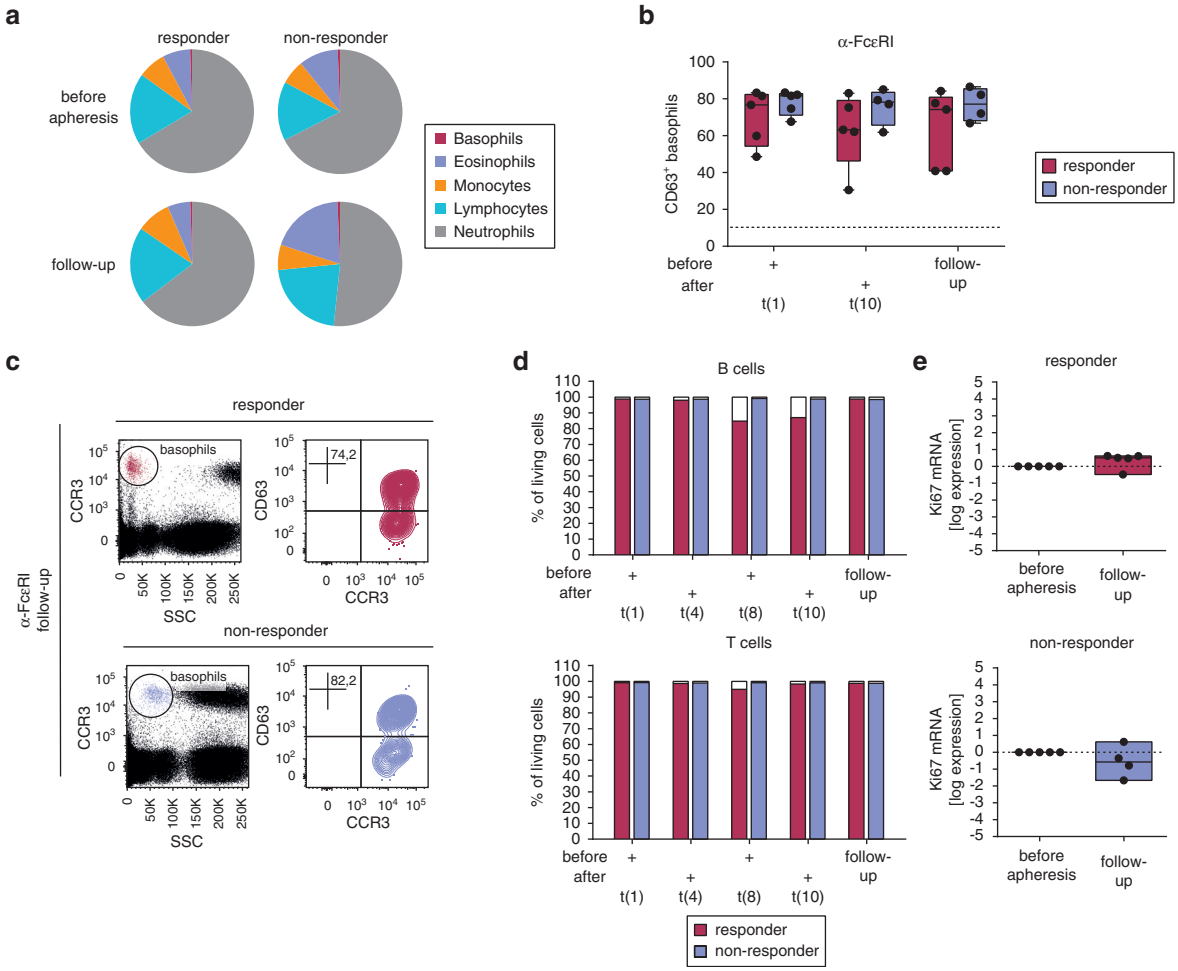

Supplementary Figure S2. Selective IgE IA does not induce immune cell death nor reduces stimulatory capacity. (**a**) Differential blood cell count as a percentage in responders (left graphs) and non-responders (right graphs) at baseline (upper row) and follow-up (lower row). (**b**) Expression of activation marker CD63 on basophils (y-axis) upon stimulation with α-FcεRI in responders (red box plots) versus non-responders (blue box plots) over time (x-axis). (**c**) Representative dot plot of one responder (red, upper graphs) and one non-responder (blue, lower graphs) of BAT. (**d**) Percentage of living B cells (upper graph) and T cells (lower graph) in responders (red) and non-responders (blue) over time as observed by flow cytometry. (**e**) RNA expression of Ki67 in PBMCs of responders (upper graph) and non-responders (lower graph). Values are normalized to baseline and shown on a logarithmic scale (y-axis). BAT, basophil activation test; IA, immune apheresis; t, time.

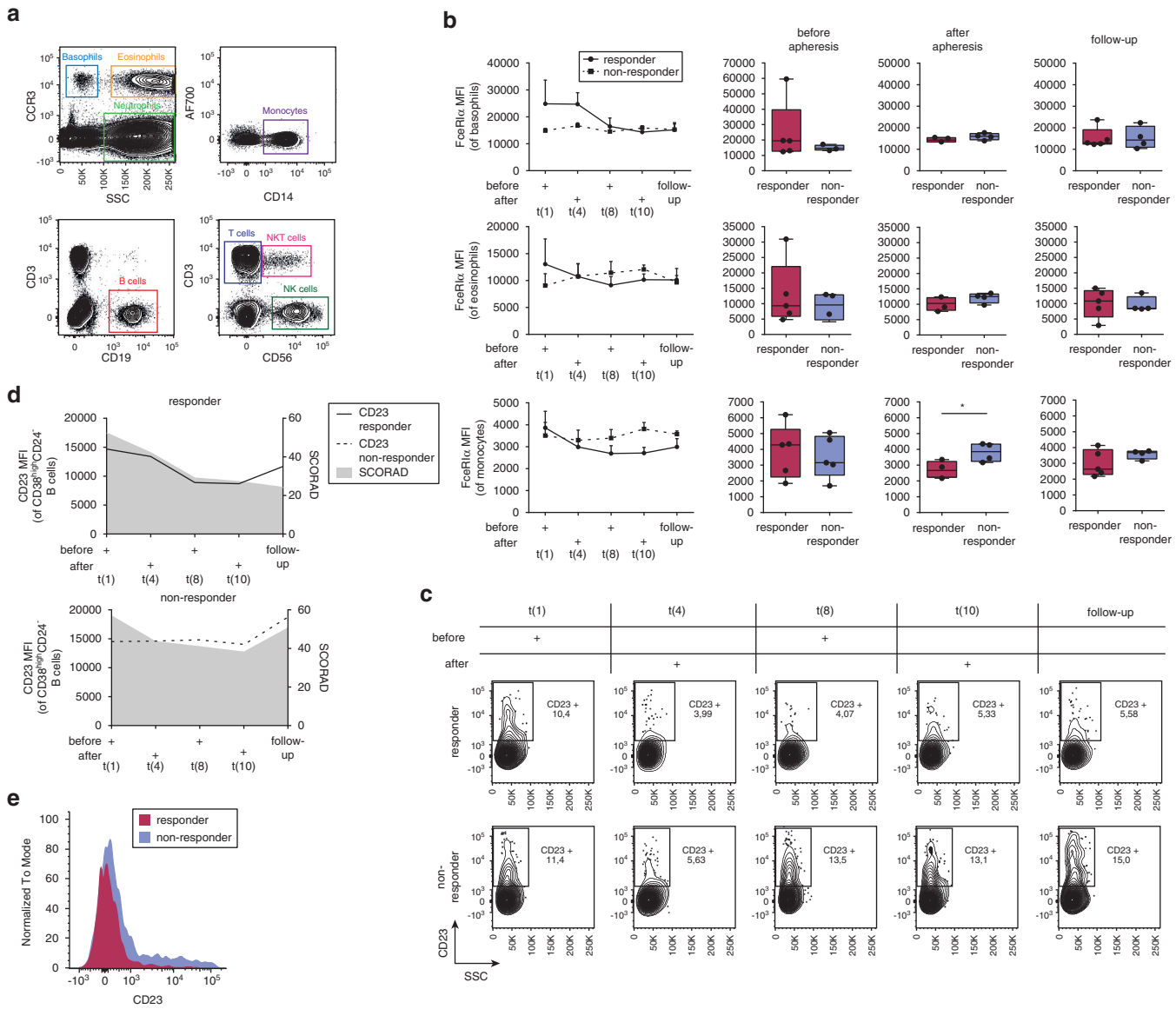

Supplementary Figure S3. Not FcεRIα levels but early and sustained downregulation of CD23 on B-cell populations predicts long-term response of selective IgE IA. (**a**) Gating strategy of peripheral immune cells. (**b**) Left graphs: FcεRIα levels on basophils (upper row), eosinophils (middle row), and monocytes (lower row) in responders (solid lines) and non-responders (dotted lines) over time. Middle and right graphs: Comparison of FcεRIα levels on basophils (upper graphs), eosinophils (middle graphs), and monocytes (lower graphs) in responders (red box plots) and non-responders (blue box plots) at baseline (middle left graphs), after last IA treatment (middle right graphs), and follow-up (right graphs). (**c**) Dot plots of CD23 levels of $CD38^{high}CD24-$ B cells in one representative responder (upper graphs) and one non-responder (lower graphs) over time (x-axis). (**d**) The course of CD23 levels on $CD38^{high}CD24-$ B cells (lines) and SCORAD (filled area) in responders (solid line, upper graph) and non-responders (dotted line, lower graph) over time (x-axis). (**e**) Mean CD23 levels of $CD38^{high}CD24-$ B cells in responders (red) and non-responders (blue) at follow-up. IA, immune apheresis; MFI, mean fluorescence intensity; NKT, NK T cell; SCORAD, scoring atopic dermatitis; SSC, side scatter; t, time.

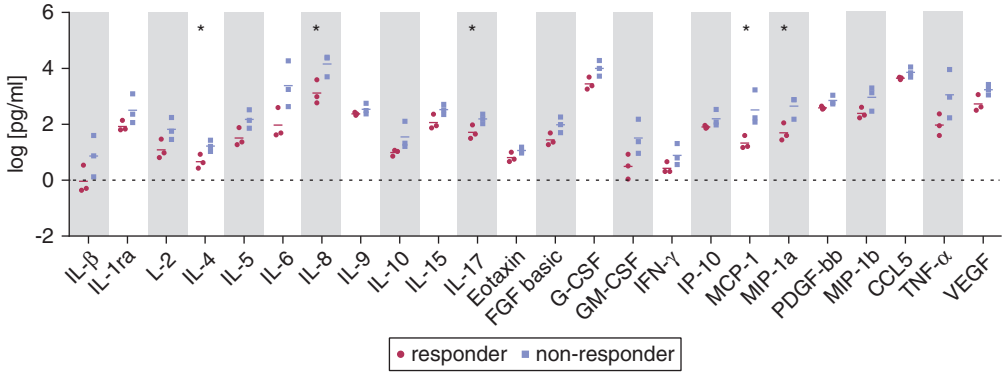

Supplementary Figure S4. Screening assay of 24 immune mediators in responders (red circles) and non-responders (blue squares) secreted by α-IgE stimulated B cells at follow-up. Y-axis shows the log transformed values.

Supplementary Table S1. Patient Characteristics

Characteristic	Pt1	Pt2	Pt3	Pt4	Pt5	Pt6	Pt7	Pt8	Pt9	Pt10	Average ± SD
Sex	M	F	M	M	M	M	F	M	M	M	
Other atopic diseases	AR, FI	AR, A	AR, A	AR, FI	AR, FI	AR, A, FI	AR	AR, A, FI	AR, A, FI	AR, A, FI	
Previous therapies	P, CS, IA + OM	P, CS	P, CS, IA + OM	PT, CS	P, CS, CYC	P, MTX, CYC, OM	P, CS, CYC	P, CS, CYC, MTX, CC	P, CS	P, CS, CYC	
Age, y	52	45	47	28	36	34	23	39	30	53	38.7 ± 10.3
Baseline SCORAD	43.4	53.1	61.4	53.9	50	47.1	51.7	40	70.9	76,1	54.8 ± 11.6
Follow-up SCORAD	20.8	26.7	27.4	29.8	16.2	54.3	42.7	44.6	62	Dropout	36.1 ± 15.6
Baseline IgE	16,211	4,918	17,657	4,759	7,487	2,329	16,232	19,796	32,236	28,694	15,031.9 ± 10,226.1
Follow-up IgE	16,206	3,834	10,929	4,781	6,180	3,280	23,424	23,259	21,102	Dropout	12,555 ± 8,550.5
Baseline DLQI	Absent	7	16	Absent	12	24	12	18	Absent	13	14.6 ± 5.4
Follow-up DLQI	Absent	2	10	7	1	21	19	5	17	Dropout	10.3 ± 7.8

Abbreviations: A, asthma; AR, allergic rhinitis; CC, Cellcept; CS, systemic corticosteroids; CYC, cyclosporin; DLQI, Dermatology Life Quality Index; F, female; FI, food intolerance; IA, immune apheresis; M, male; MTX, methotrexate; O, omalizumab; Pt, patient; P, phototherapy; SCORAD, scoring atopic dermatitis.